JAST, Vol. 6, No. 2, pp 87–97
◯ Iranian Aerospace Society, Spring 2009

JAST
Journal of Aerospace Science and Technology

An Experimental Study of Heat Transfer around a Cylinder in Presence of Electric Field

S. Reza-zadeh[1], H. Masumi[2], E. Esmaeilzadeh[3]

In this paper, effects of EHD actuators on hydrodynamic behavior and heat transfer of air flow over a circular cylinder were considered. Pressure and temperature distributions around the cylinder were measured in presence of wire-plate EHD actuators. The Reynolds number based on cylinder diameter (d) were 3500, 7000. Experiments were performed for various configurations. Based on the obtained results, the flow field around the cylinder was affected significantly by EHD actuation. The flow visualization confirmed the formation of separation bubble because of EHD actuation and affected pressure distribution dramatically. Measured temperatures showed that the excess flow, resulted from corona wind, enhanced local and average heat transfer over the cylinder.

NOMENCLATURE

A_S	Cylinder surface (m^2)
C_p	Pressure coefficient
C_d	Drag coefficient
d	Diameter of cylinder(m)
D_p	Pressure drag force (N)
EHD	Electrohydrodynamic
H	Distance between wire electrode and the cylinder
L	Length of cylinder (m)
Nu	Nusselt number
Nu_0	Nu number for leading edge without EHD actuation
$\overline{Nu}$	Average Nu number over the cylinder surface
P	Pressure (N/m^2)
P_0	Ambient pressure (N/m^2)
R	Radius of cylinder (m)
Re	Reynolds number based on diameter
U_0	Velocity of mainstream (m/s)

Greek symbols

α	Angle of wire electrodes form leading edge in clockwise direction
θ	Angle over the cylinder from leading edge in clockwise direction
Δt	Time step(s)

INTRODUCTION

The fluid flow around a cylinder has been investigated by many researchers and scientists due to complicated behavior such as vortex shedding phenomenon and flow separation behind the cylinder. They applied some methods and devices to control this flow and optimize the design. Most of these techniques have been concentrated on Boundary layer and wake zone and have been used to change them to obtain the best efficiency.

These methods have been divided into three groups: (1) passive control, (2) active control and (3) compound control. Passive control techniques do not need any external energy during controlling. Additional devices in the fluid flow or modified geometry of the bluff body such as splitter plate, base bleed, roughness elements, ... are used. Active control techniques such as EHD actuators and vibrators need external energy to change fluid flow.

The application of electrohydrodynamic (EHD) actuators was reported some decades ago. EHD corresponded to the interaction of electric and flow fields. High field strength in the vicinity of sharp

1. *(Corresponding Author), Ph.D. Candidate, Dept. of Mech. Eng., Univ. of Tabriz, Tabriz, Iran.*
2. *MSc. Student, Dept. of Mech. Eng., Univ. of Tabriz, Tabriz, Iran.*
3. *Professor, Dept. of Mech. Eng., Univ. of Tabriz, Tabriz, Iran, Email:esmzadeh@tabrizu.ac.ir.*

emitter produces ions and accelerates them to opposite electrode. Energy transfer between charges and fluid molecules leads to flow motion which is called ionic wind or corona wind.

The Corona wind phenomenon was reported by Hauksbee [1] in 1719. Then, chattok.1899, Steutzer.1959, Robinson.1961, Velkoff.1968, yabe.1978, Rosendal.1988, Crowly.1990, Semoto.1992, Ohadi.1991, and Seyed-Yaghoobi. 1991. 1992. 1995. 2003 used this phenomenon for various applications and extended it. Leger *et.al.* [2,3] could reduce wake zone behind a plate by EHD actuators and found out that the kinetic energy induced by the ionic wind inside the boundary layer allows a drag reduction for low Reynolds numbers. Artana *et.al.* [4] investigated the fluid flow around a cylinder by wire plate electrodes and modified the size of mean recirculation region behind the cylinder. Hyun *et.al.* [5] performed some experiments to investigate the effect of distance between electrodes. They found out the wake structure behind the cylinder and concluded that pressure drag can be affected by imposing corona wind. On-set of EHD turbulence was reported by Chang *et.al.* [6] in cross flow around a cylinder. They generated EHD turbulence even at very low Re numbers. Jukes *et.al.* [7] used dielectric barrier discharge (DBD) plasma actuator to control flow around a cylinder.

The above studies focused on electrohydrodynamic behavior, but in the present work, EHD actuation as an active control method is applied to control heat transfer and hydrodynamic behavior around the cylinder. In this approach, wire-plate electrodes are used as EHD actuators. Experiments were performed to examine various electrode configurations. $\alpha = 0°$, $\pm 30°$, $\pm 90°$, $\pm 150°$, $\pm 180°$, $H = R$, $R/2$, $R/3$ at $Re = 3500$, 7000. Pressure and temperature were measured to study flow patterns and heat transfer in every case.

EXPERIMENTAL SET-UP

Wind–tunnel facilities

Experiments were carried out in an open-circuit subsonic wind tunnel which is illustrated in Figure 1a,b,c. The settling chamber contained a honeycomb and then a 4.9 to 1 contraction cone. The contraction cone led to the test section, which was a rectangular 0.43×0.43m duct 1.28 m long. The walls of the channel were made of 5 mm thick Plexiglas. The mainstream flow was generated by a variable speed axial fan at the end of diffuser. The fan was driven by 7kW motor with a maximum speed of 3000 rpm. Two mainstream velocities of 1 m/s and 2 m/s are studied. Free stream turbulence is 0.5%. Figure 1a,b,c shows the wind tunnel and schematic diagram of the experimental set-up.

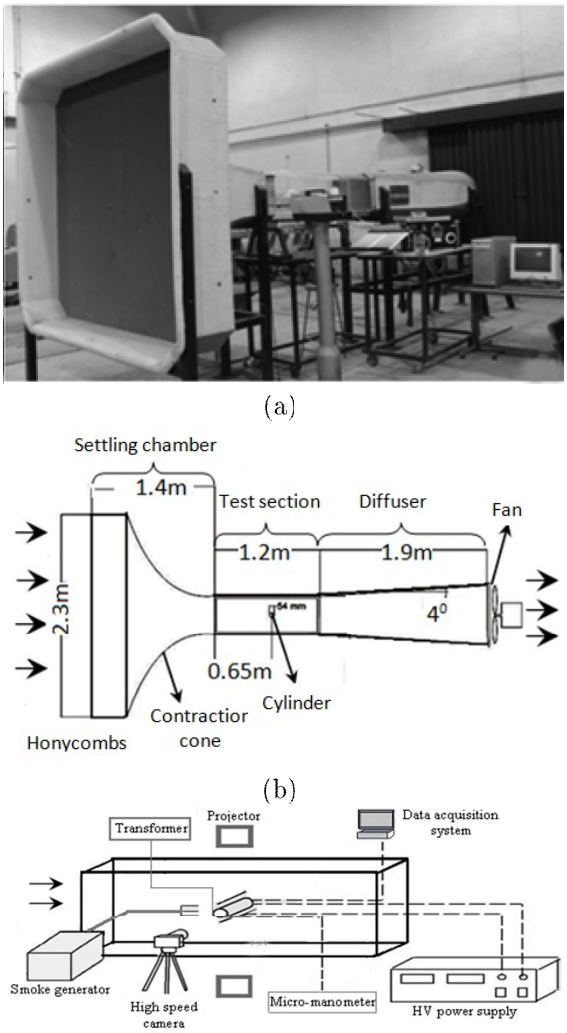

Figure 1. Experimental set-up: (a) open-circuit subsonic wind tunnel, (b) geometry of wind tunnel, (c) schematic diagram of experimental setup.

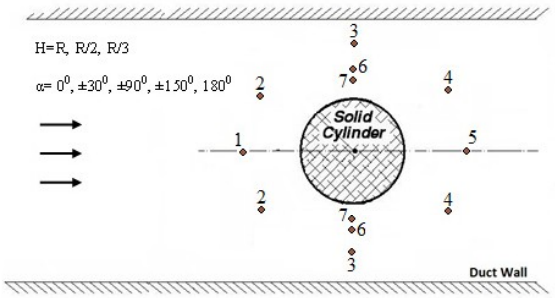

Figure 2. Arrangments of electrods.

Cylinder and wires configurations

A smooth cupper circular cylinder with an outer diameter of $D = 5.4$ cm, an inner diameter of $D = 5.0$ cm, and a length of $L = 44$ cm was positioned horizontally,

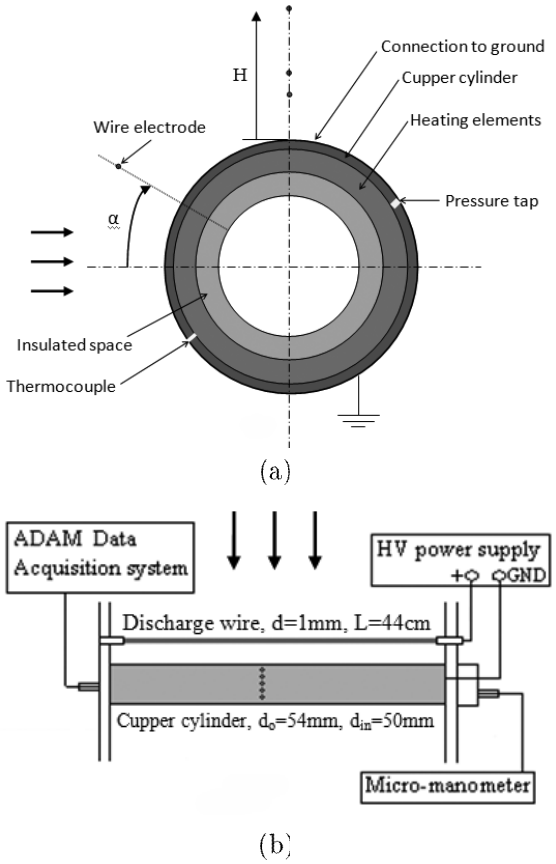

Figure 3. The schematic model of cylinder, (a) side view; (b) top view.

spanning the axis normal to the flow. The Cupper wires with a diameter of $d = 1$ mm were used as positive discharge electrodes that were located symmetrically and parallel to the axis of the cylinder with spacing $H = R, R/2, R/3$ as shown in Figure 2.

Surface thermal mapping by thermocouples and pressure measurements

The free stream air was maintained at ambient temperature. The cylinder was heated by an 220Ω-heating element which generated a constant heat flux. In order to protect pressure tubes and thermocouples, the space between the heater and pressure, thermocouples devices were insulated. 19 pressure taps and 19 iron/Constantan (J type) thermocouples were embedded at 10° intervals on the cylinder. All measurements were done for the upper half of the cylinder because of symmetrical shape. The output of the thermocouples was connected to ADAM data acquisition system. The pressure was measured by micro manometer (Furness controls, LTD). The side and top view of the cylinder is illustrated in Figure 3a,b. The side view is enlarged.

To explain heat transfer and hydrodynamic behavior, we considered dimensionless variables such as C_p (pressure coefficient), C_d (pressure drag coefficient) and Nu (heat transfer coefficient) that were defined as below:

$$C_p = \frac{2(p - p_0)}{\rho U_0^2} \tag{1}$$

$$C_d = \frac{2D_p}{\rho U_0^2 A_S} \tag{2}$$

$$Nu = \frac{hd}{k} \tag{3}$$

$$\overline{Nu} = \frac{\bar{h}d}{k} \tag{4}$$

where ρ was the air density, P_o and U_0 were static pressure and velocity of free mainstream respectively, h and P were heat transfer coefficient and pressure on the surface of the cylinder respectively. D_p was the component of pressure drag in the flow direction, d was cylinder diameter, A_s was area, and k was heat conductivity of air.

For drag over the cylinder, we just considered the variation of pressure drag because friction drag wasn't considerable. Friction drag for $Re = 3500$ and 7000 are 7.82% and 5.66% of total drag respectively, as Khan et al [8] explained analytically for laminar flow. A correlation based on Block Ratio (BR) [9] was performed for C_d.

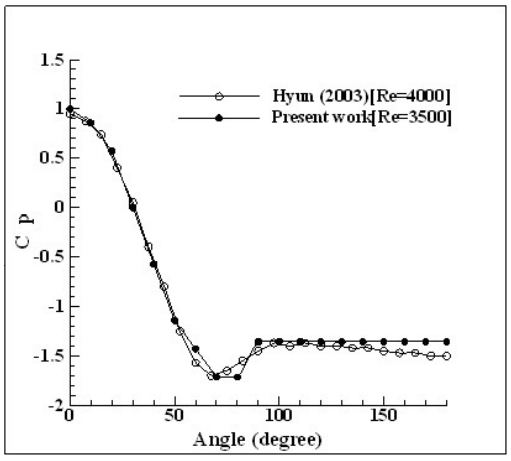

Figure 4. Arrangments of electrods.

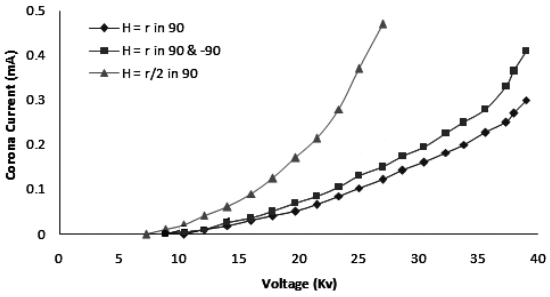

Figure 5. Corona current versus applied voltage.

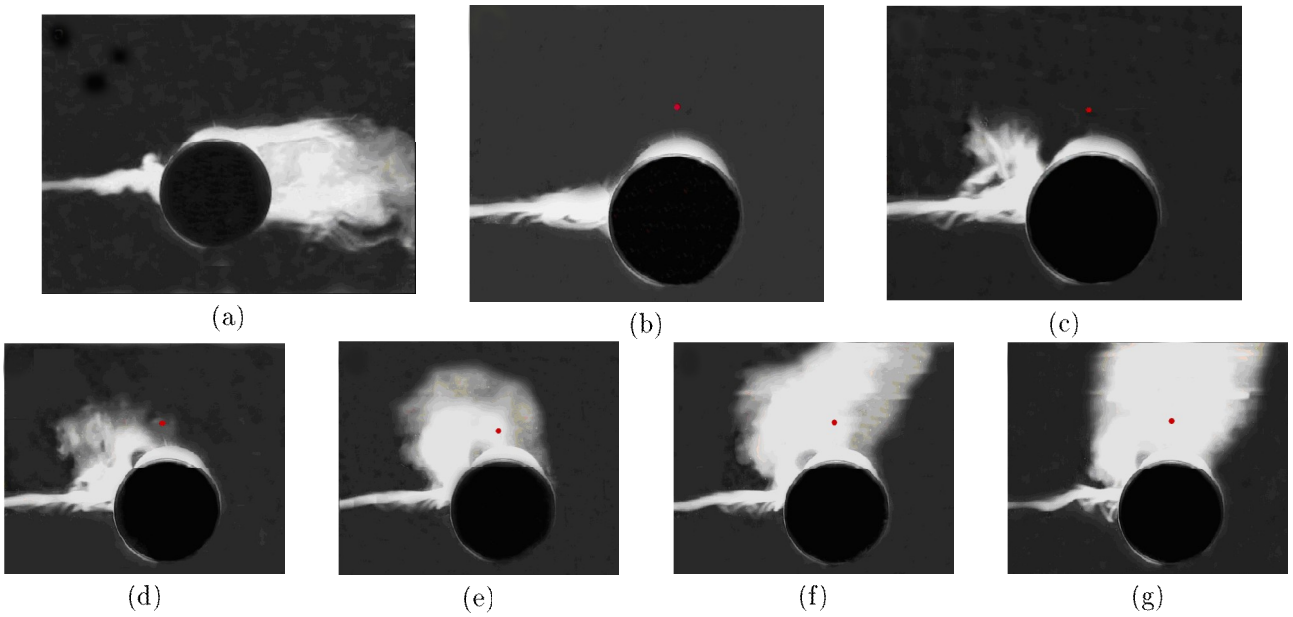

Figure 6. flow visualization, $\alpha = 90$, $H = R$, (a) no EHD, (b-g) with EHD,V_{app}=30 KV, $\Delta t = 0.03s$.

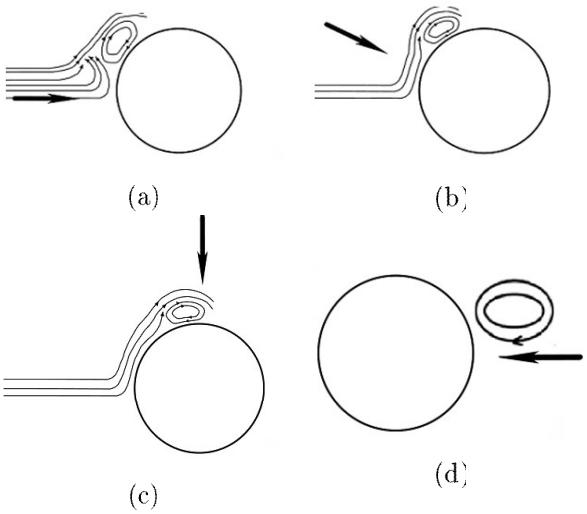

Figure 7. Schematic digaram of fluid flow for α=0^0,$\pm 30^0$,$\pm 90^0$,180^0.

Flow visualization technique

Flow visualizations were performed using a smoke generator system at a free stream velocity of 0.5 m/s. Smoke was led to the cylinder by a glass pipe with a diameter of d = 6mm. It was located 10D upstream from the cylinder. Flow pattern images were captured by a digital camera (Casio Exlim ExF1).

Electrical properties of the DC corona discharge

Corona wind was generated by wire-plate actuators. Wires as anode electrodes were connected to high-voltage (0-40Kv) DC power supply with a positive polarity. The cylinder was connected to the ground and acted as Cathode electrodes. Accuracy of the measured current and applied voltage are ± 2.5% and ± 2% respectively.

RESULTS AND DISCUSSION

For evaluation of experiments, a comparison of the pressure coefficient for the present work and another study is presented in Figure 4.

Four corona discharge regimes appeared by increasing applied voltage: spot type, glow regime, streamer and spark regime. The glow regime was suitable as a means of flow control [5], so we undertook a study of this regime. Figure 5 shows the current-voltage curves for these cases: (1) a single wire electrode was placed at $\alpha = 90$ and $H = R$, (2) a pair of wire electrodes were used at $\alpha = \pm 90$ and $H = R$, and (3) a single wire electrode was at $\alpha = 90$ and $H = R/2$. The corona onset voltages were 10.38kV, 8.86 kV and 7.2kV respectively. It could be observed that corona onset voltage increased by increasing H.

Images of flow patterns for a case at Re = 1000 were shown in Figure 6(a-g). Figure 6a illustrates flow around the cylinder without EHD actuation and Figure 6(b-g) presents flow with actuation in various time intervals. They show that, by applying EHD, flow over the cylinder was affected and a recirculation zone appeared. Effects of this separation bubble will be discussed for each case.

Flow patterns for α = 0°, 30°, 90°, 180° are presented schematically in Figure 7(a-d).

Experimental uncertainties were calculated on the

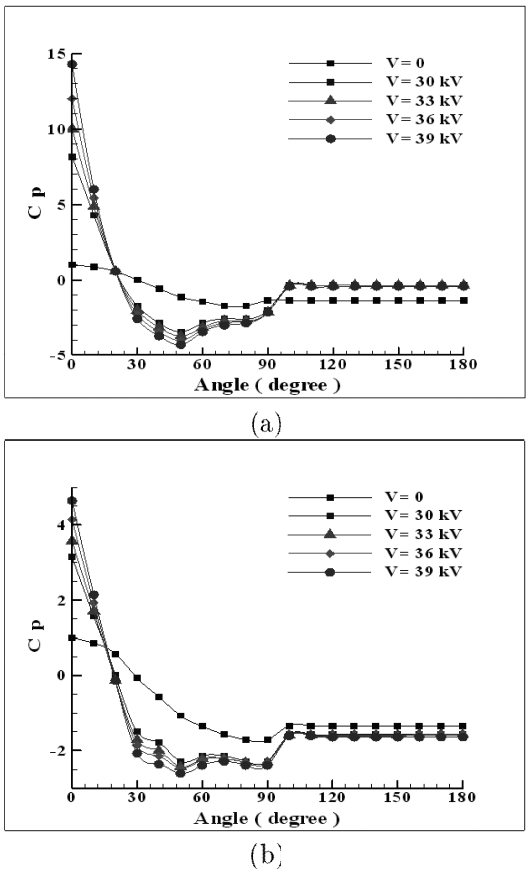

Figure 8. pressure distribution over the cylinder surface, $\alpha = 0$: (a) $Re = 3500$ (b) $Re = 7000$.

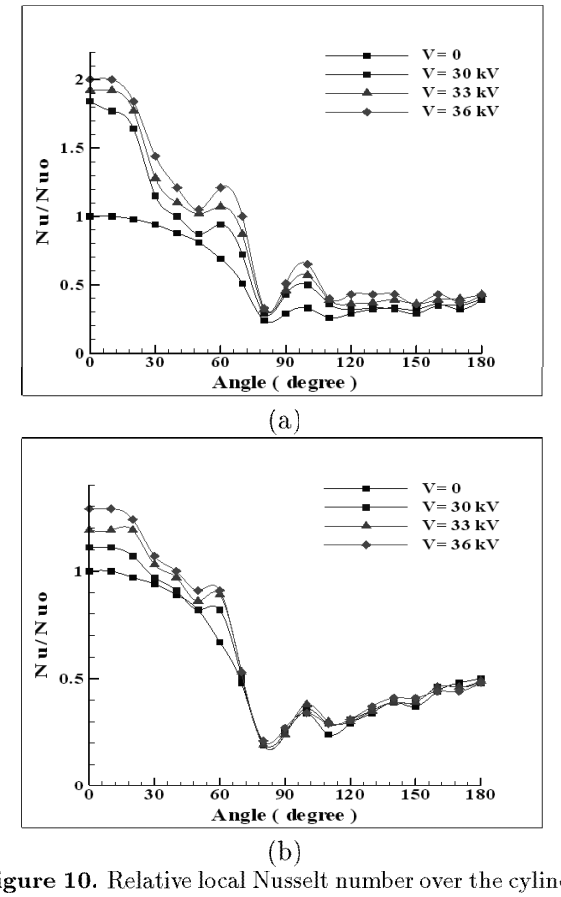

Figure 10. Relative local Nusselt number over the cylinder surface, $\alpha = 0$: (a) $Re = 3500$ (b) $Re = 7000$.

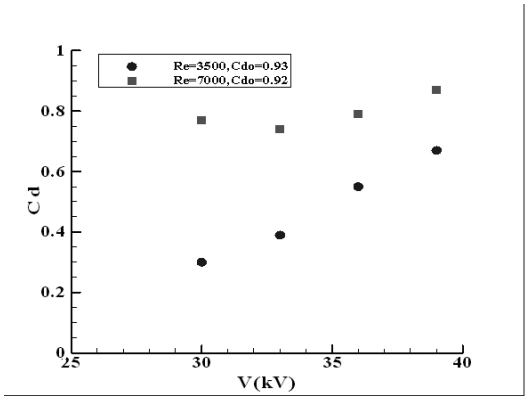

Figure 9. Pressure drag cofficient versus applied voltage, $\alpha = 0$.

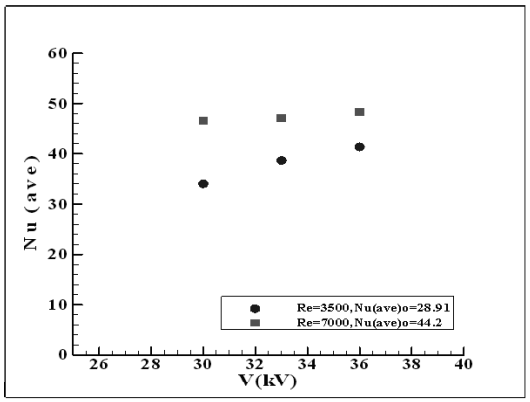

Figure 11. Average Nusselt number versus applied voltage, $\alpha = 0$.

basis of the partial derivative method of Moffat [10]. In accordance with uncertainties of ±1% for applied voltage, ±2.5% for current and 1^0C for temperature, the maximum percent of uncertainty for Nu number was 0.64%.

Figure 8a,b show distribution of pressure coefficient C_p over the cylinder for various applied voltage with two different Re numbers, 3500 and 7000. Angle of wire electrode from leading edge α was zero and wire was placed at $H = R$. As shown in Figure 8a, C_p had a large amount at $\theta = 0$. Then it decreased and reached a minimum value at $\theta = 50$. Fluid field around the cylinder in this case is shown schematically in Figure 7a. Wire electrode at $\alpha = 0$ caused a strong excess flow toward the cylinder by corona wind which increased pressure in region θ=0~20°. Beyond the

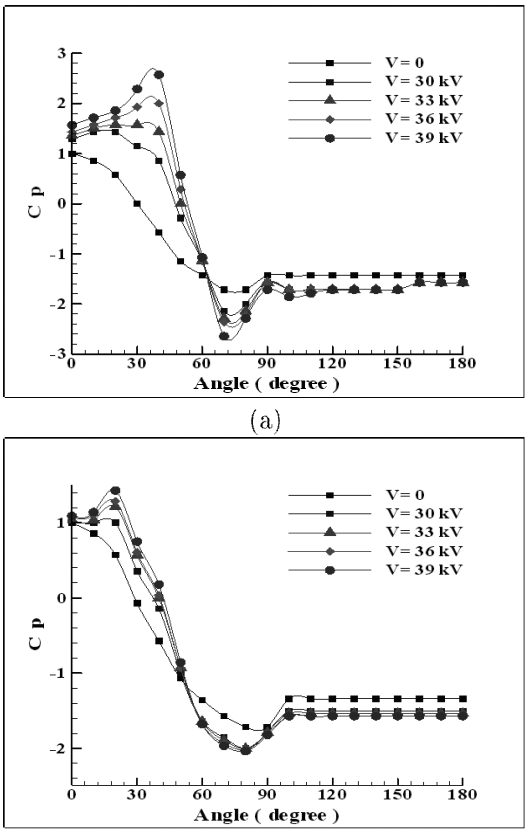

Figure 12. pressure distribution over the cylinder surface, $\alpha = 30$: (a) $Re = 3500$ (b) $Re = 7000$.

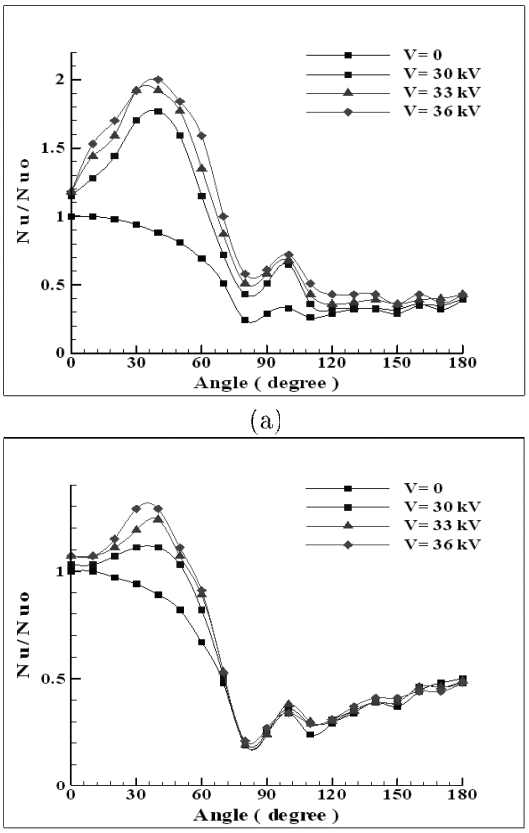

Figure 14. Relative local Nusselt number over the cylinder surface, $\alpha = 30$: (a) $Re = 3500$ (b) $Re = 7000$.

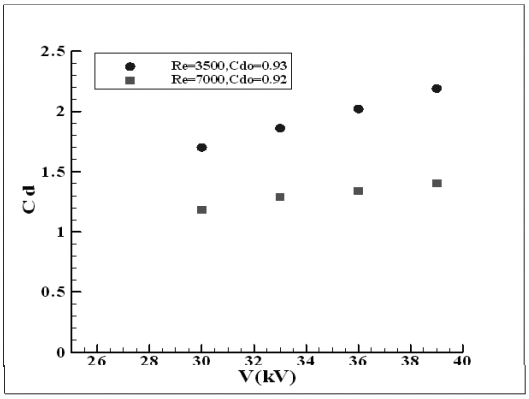

Figure 13. Pressure drag cofficient versus applied voltage, $\alpha = 30$.

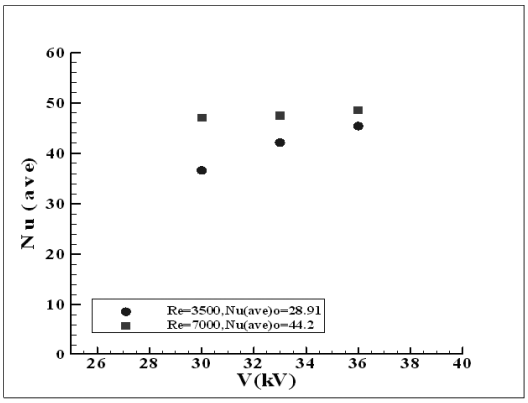

Figure 15. Average Nusselt number versus applied voltage, $\alpha = 30$.

$\theta = 20°$, the excess flow tends to separate but the main flow, because of its high momentum flux, causes recirculation zone and generates the separation bubble on the cylinder surface. This phenomenon led C_p to drop. Beyond the recirculation zone, mainstream over the cylinder behaved as a normal case (without EHD actuation) and caused tc increase C_p gradually. Separation happened at $\theta = 80$ and behind the cylinder C_p increased for low Re number. Although for $Re = 300$, EHD actuation increased local velocity at the leading edge but for $Re = 7000$, the effect of actuation at $\alpha = 0$ behind the cylinder wasn't considerable. In Figure 9, drag coefficient C_d for $Re = 3500$, 7000 at various applied voltage is shown. C_d increased by increasing applied voltage because of increasing vortices of the separation bubble. Figure

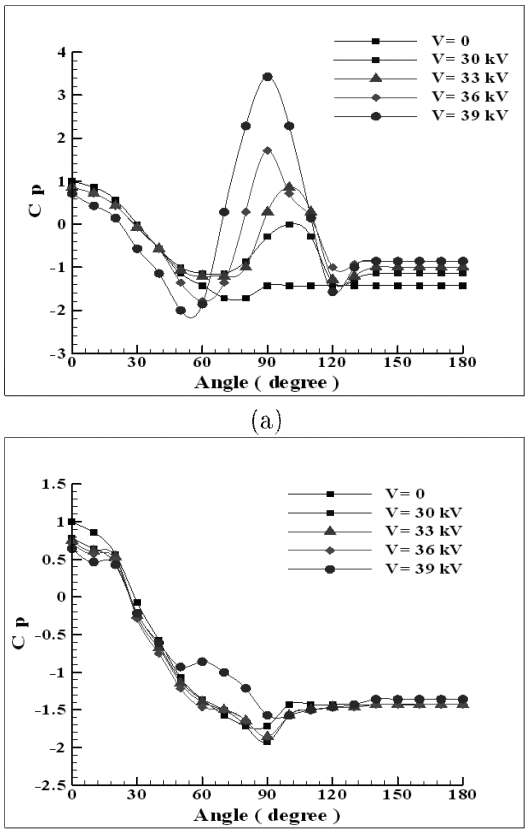

Figure 16. Pressure distribution over the cylinder surface, $\alpha = 90$: (a) $Re = 3500$ (b) $Re = 7000$.

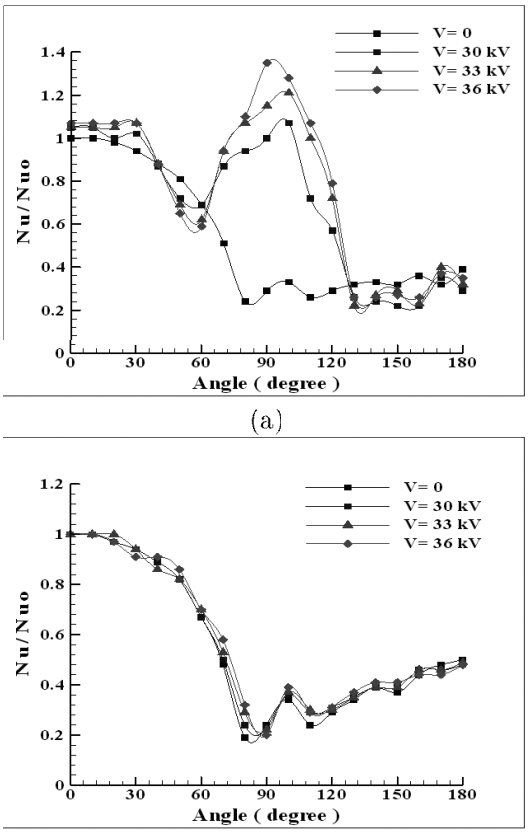

Figure 18. Relative local Nusselt number over the cylinder surface, $\alpha = 90$: (a) $Re = 3500$ (b) $Re = 7000$.

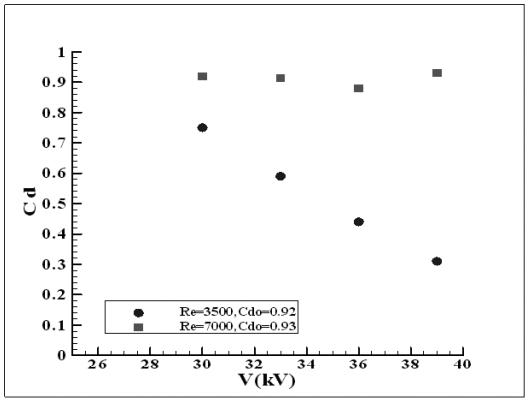

Figure 17. Pressure drag cofficient versus applied voltage, $\alpha = 90$.

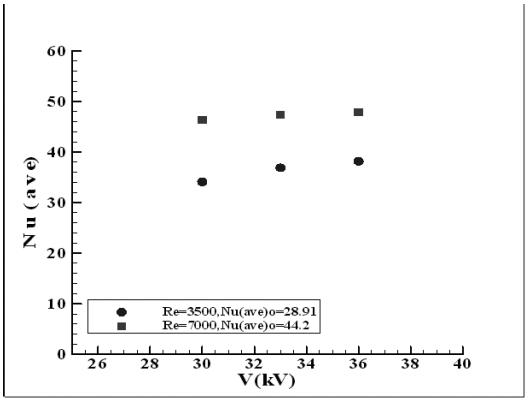

Figure 19. Average Nusselt number versus applied voltage, $\alpha = 90$.

10a,b illustrates relative local Nusselt number over the surface of the cylinder for various applied voltage at $Re = 3500, 7000$ respectively. Nu/Nu_o increased at $\theta = 0$ because of excess flow. Momentum of the excess flow increased by increasing applied voltage. The minimum and maximum, observed in Figure 10a, confirm the presence of the separation bubble. In comparison with a normal case, Nu/Nu_o behind the cylinder is greater. For $Re = 7000$, the effect of EHD actuation was negligible behind the cylinder. Figure 11 shows the average Nu number ($\overline{Nu}$) for $Re = 3500, 7000$ at various applied voltage respectively. The average Nu number increased by increasing applied voltage.

At $\alpha = \pm 30°$, Figure 12a, b shows C_p around the cylinder. As it is shown, it was maximum in region θ=30~40. Fluid flow around the cylinder in this case

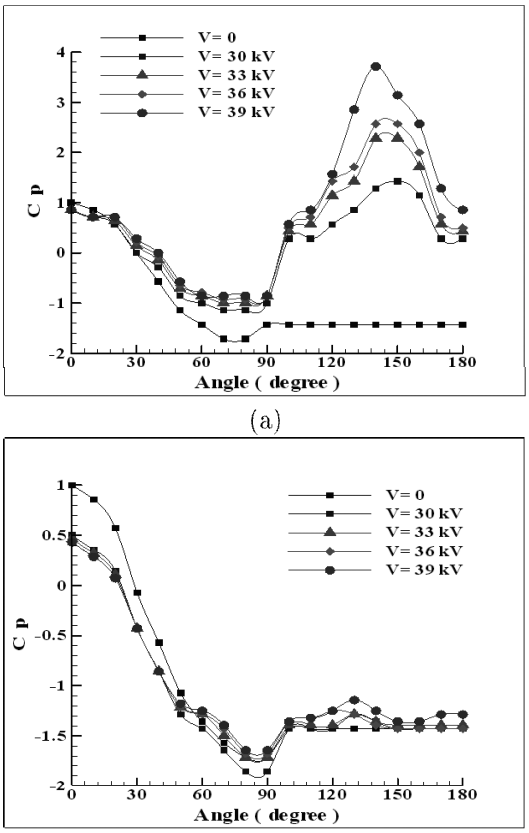

Figure 20. pressure distribution over the cylinder surface, $\alpha = 150$: (a) $Re = 3500$ (b) $Re = 7000$.

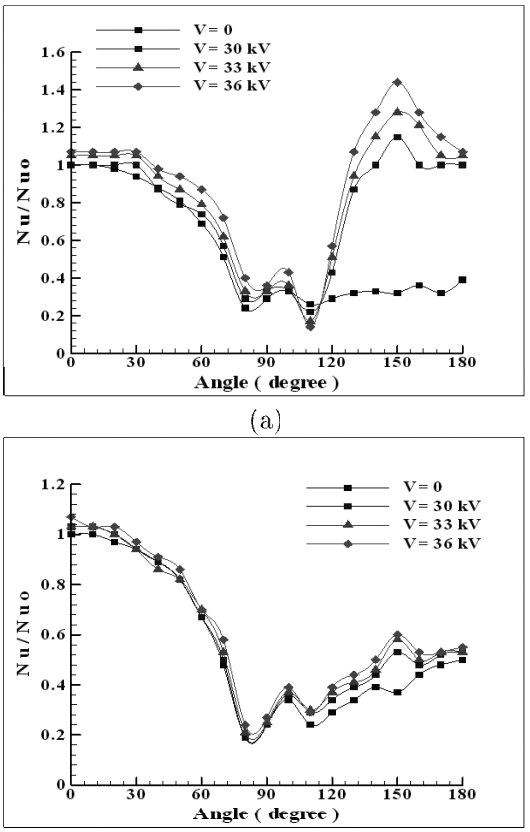

Figure 22. Relative local Nusselt number over the cylinder surface, $\alpha = 150$: (a) $Re = 3500$ (b) $Re = 7000$.

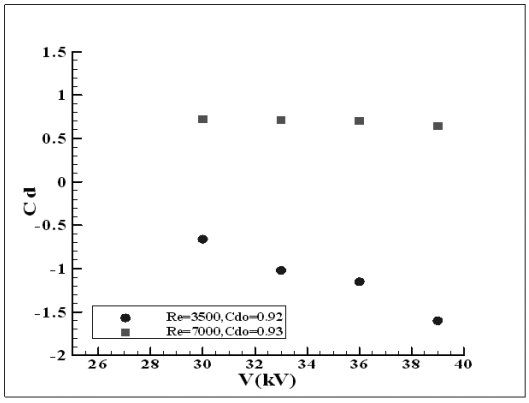

Figure 21. Pressure drag cofficient versus applied voltage, $\alpha = 150$.

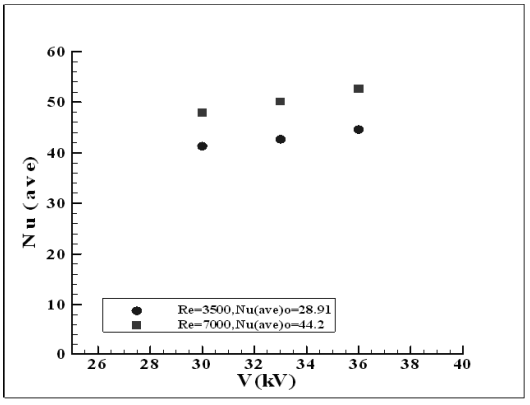

Figure 23. Average Nusselt number versus applied voltage, $\alpha = 150$.

is shown schematically in Figure 7b. Beyond $\theta = 30$, as mentioned before, the formation of separation bubble led C_p to drop. Figure 13 shows drag coefficient for $Re = 3500$, 7000. C_d increased by increasing applied voltage. Nu/Nu_o for this case is shown in Figure 14a, b. In region θ=30~40, Nu/Nu_o was a maximum because of corona wind. Then, a minimum was observed because of mainstream separation. $\overline{Nu}$ is illustrated in Figure 15. Average Nu number increased by increasing applied voltage.

Figure 16a, b shows C_p for $Re = 3500$, 7000 respectively. Wire electrodes were placed at $\alpha = \pm 90°$. As shown, it reached a maximum value at $\theta = 90$. Fluid flow around cylinder is shown schematically in Figure 7c. EHD actuation at $\alpha = 90$ caused the separation bubble reattached at $\theta = 90$ and separation

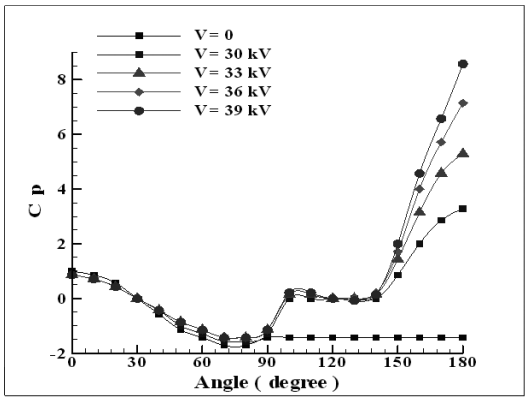

(a)

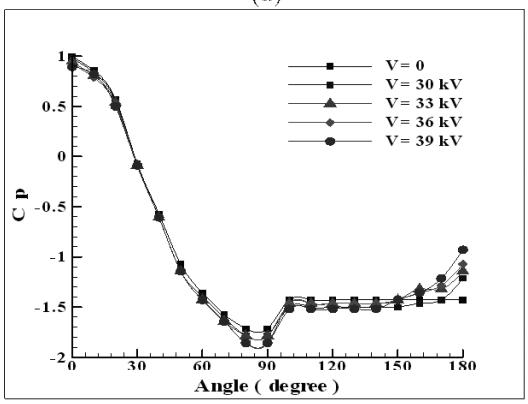

(b)

Figure 24. pressure distribution over the cylinder surface, $\alpha = 180$: (a) $Re = 3500$ (b) $Re = 7000$.

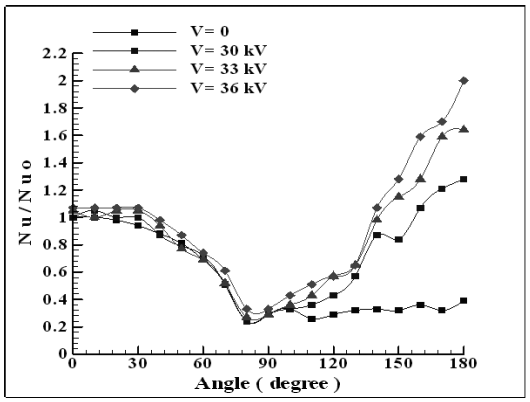

(a)

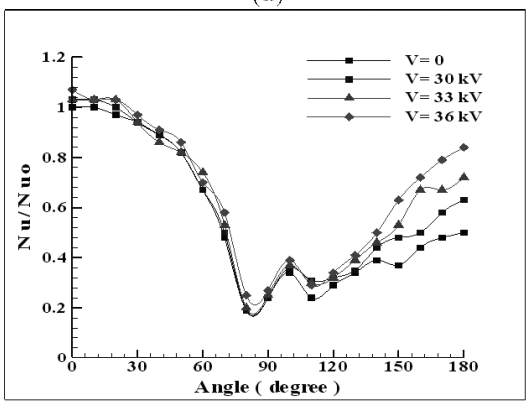

(b)

Figure 26. Relative local Nusselt number over the cylinder surface, $\alpha = 180$: (a) $Re = 3500$ (b) $Re = 7000$.

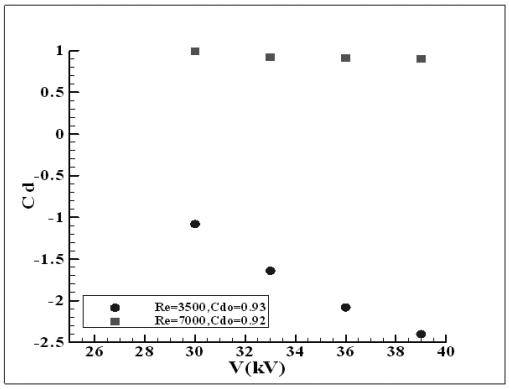

Figure 25. Pressure drag cofficient versus applied voltage, $\alpha = 180$.

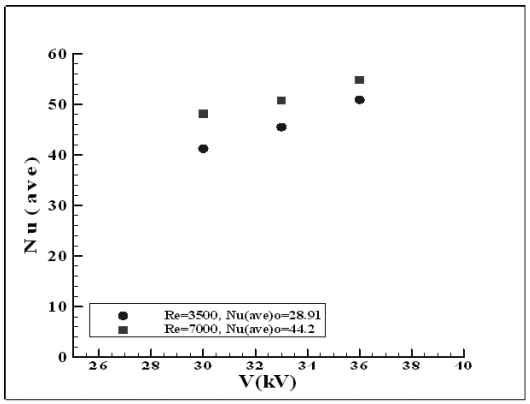

Figure 27. Average Nusselt number versus applied voltage, $\alpha = 180$.

of mainstream delayed. In comparison with normal a case. C_p behind the cylinder was greater. For strong corona wind, maximum C_p (reattachment point) was at $\theta = 90$ but for weak corona wind, it was at $\theta > 90$ because of mainstream flow. In Figure 17, C_d is shown for $Re = 3500$, 7000 respectively. The effect of EHD actuation wasn't considerable for $Re = 7000$ whereas C_d decreased by increasing applied voltage for Re=3500 because the separation bubble reattachment tended to $\theta = 90$. Figure 18a, b shows Nu/Nu_c in this case. Both diagrams have a minimum and a maximum that correspond to the separation bubble and its reattachment. Behind the cylinder, in comparison with a normal case, Nu/Nu_c was less than the normal case because separation was delayed. $\overline{Nu}$

is shown in Figure 19. Average Nu number increased by increasing applied voltage.

Figure 20a, b shows C_p for $Re = 3500$, 7000 respectively. EHD actuators were placed at $\alpha = \pm 150°$. C_p at stagnation point was less than a normal case because the corona wind was against the mainstream flow. Separation happened in region θ=80~90 and pressure increased and reached a maximum about $\theta = 150$ behind the cylinder. In Figure 21, drag coefficient is shown. For $Re = 7000$, variation wasn't considerable whereas C_d decreased by increasing applied voltage even when it was less than zero for $Re = 3500$. For $Re = 3500$, corona wind affected the wake zone but for $Re = 7000$, the mainstream had high momentum flux and corona wind couldn't be effective. Figure 22a, b shows Nu/Nu_o for this case. By EHD actuation at $\alpha = 150$, heat transfer increased behind the cylinder because of excess flow. Figure 23 illustrates $\overline{Nu}$. Average Nu number increased by increasing applied voltage.

Figure 24a, b shows C_p with EHD actuation at $\alpha = 180$. As shown, C_p at stagnation point wasn't affected but reached a maximum value at $\alpha = 180$ behind the cylinder. The behavior of flow around cylinder is shown schematically in Figure 7d. In Figure 25, drag coefficient is shown. For $Re = 7000$, variation was not considerable whereas C_d decreased by increasing applied voltage even when was less than zero for Re=3500, because the corona wind was against mainstream flow. Figure 26a, b shows Nu/Nu_o for this case. By EHD actuation at $\theta = 180$, heat transfer increased behind the cylinder because of corona wind behind the cylinder. Figure 27 illustrates $\overline{Nu}$. Average Nu number increased by increasing applied voltage because vortices were strengthened by corona wind.

To investigate the effects of H variation, Figure 28, 29 shows C_p with EHD actuation at $\alpha = 90$ and $Re = 3500$ for two different $H = R/2$, $R/3$ (The effect of EHD at $Re = 7000$ wasn't considerable). As shown, C_p reached a maximum value about $\alpha = 90$ because of EHD actuation. By considering C_p for applied voltage 24KV and 23KV in Figure 28, 29, respectively, we found (1) for $H = R/3$ the effect of EHD actuation was stronger than $H = R/2$ (maximum C_p was greater), (2) for $H = R/3$, reattachment happened at $\theta = 90$ in comparison with $H = R/2$ which happened at $\theta = 100$. Figure 30, 31 shows Nu/Nu_o for these distances. Comparison of Nu/Nu_o at applied voltage 24KV and

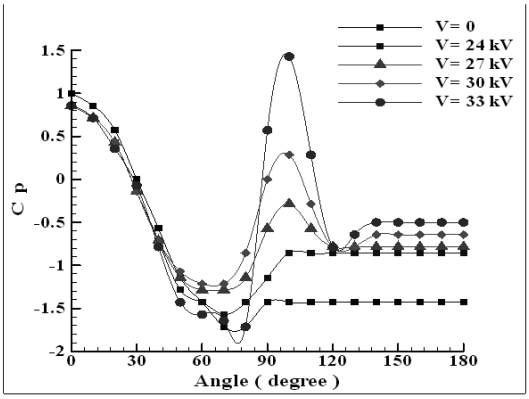

Figure 28. Pressure distribution over the cylinder surface, $\alpha = 90$, $H = R/2$, $Re = 3500$.

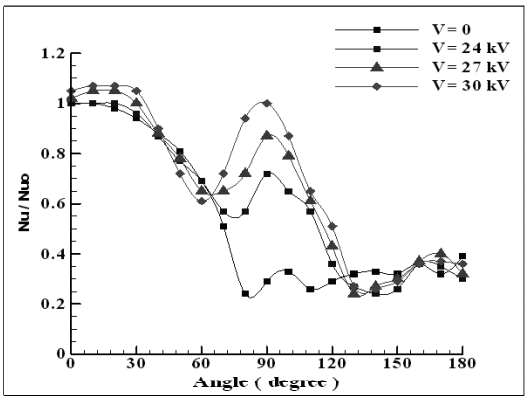

Figure 30. Relative local Nusselt number over the cylinder surface, $\alpha = 90$, $H = R/2$, $Re = 3500$.

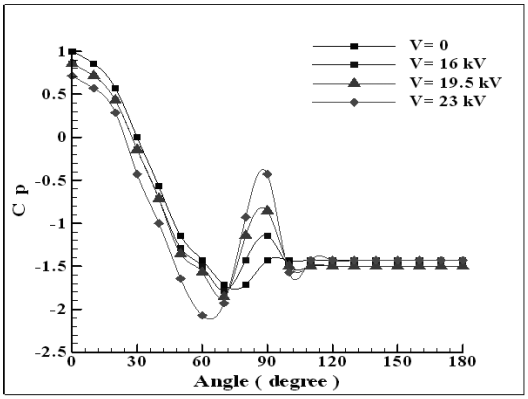

Figure 29. Pressure distribution over the cylinder surface, $\alpha = 90$, $H = R/3$, $Re = 3500$.

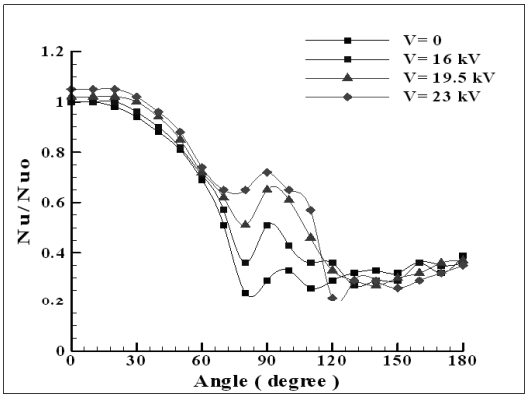

Figure 31. Relative local Nusselt number over the cylinder surface, $\alpha = 90$, $H = R/3$, $Re = 3500$.

23KV in Figure 30, 31, respectively, shows variation of heat transfer was not significant.

CONCLUSION

Flow around a circular cylinder in presence of EHD actuation was studied for various configurations of electrodes. Experiments were undertaken for two Re numbers $Re = 300$, 7000. The formation of separation bubble was observed in presence of corona wind and its position depended on the wire electrodes angle (α). The pressure coefficient was affected dramatically by this bubble. So, it could be a suitable means for controlling drag coefficient.

For cases $\alpha = \pm 150^{\circ}$, $= \pm 180^{\circ}$, C_d was less than zero because of the large recirculation zone behind the cylinder.

When $\alpha = \pm 90^{\circ}$, the separation of mainstream was delayed, and heat transfer decreased by increasing applied voltage. But for corona wind against mainstream flow, for cases $\alpha = \pm 150^{\circ}, = \pm 180^{\circ}$ it increased because of increment of vortices. The corona wind could generate excess flow which enhanced local and average heat transfer.

REFERENCES

1. Hauksbee F., *Physico-Mechanical Experiments on Various Subjects*, London, PP 46-47(1719).
2. Leger L., Moreau E., Artana G., Touchard G., "Influence of a DC Corona Discharge on the Airflow along an Inclined Flat Plate", *J. Electrostatics*, **50**(51), PP 300-306(2001).
3. Leger L., Moreau E., Gerard G., Touchard G., "Effect of a DC Corona Electrical Discharge on the Airflow along a Flat Plate", *IEEE Transactions on Industry Applications*, **38**, PP 1478-1485(2002).
4. Artana G., Sosa R., Moreau E., Touchard G., "Control of the Near-Wake Flow around a Circular Cylinder with Electrohydrodynamic Actuators", *Experiment in Fluids*, **36**, PP 580-588(2003).
5. Hyun K.T., Chun C.H., "The Wake Flow Control Behind a Circular Cylinder Using Ion Wind", *Experiments in Fluids*, **35**, PP 541-552(2003).
6. Chang J.S., Brocilo D., Urashima K., Dekowskib J., Podlinskib J., "On-Set of EHD Turbulence for Cylinder in Cross Flow under Corona Discharges", *Journal of Electrostatics*, **64**, PP 569-573(2006).
7. Jukes T.N., Choi K.S., "Flow Control around a Circular Cylinder using Pulsed Dielectric Barrier Discharge Surface Plasma", *Physics of Fluids*, **21**, (2009).
8. Khan W.A., Culham J.R., Yovanovich M.M., "Fluid Flow and Heat Transfer from Elliptical Cylinders: Analytical Approach", *37th AIAA Thermophysics Conference, AIAA 2004-2272*, PP 1-11(2004).
9. Ota T., Okamoto Y., Yshikawa H., "A Correction Formula for Wall Effects on Unsteady Forces of Two-Dimensional Bluff Bodies", *J. Fluids Eng.*, **12**, PP 414-418(1994).
10. Moffat R.J., "Describing the Uncertainties in Experimental Results", *Experimental Thermal and Fluid Science*, **1**, PP 3-17(1988).